

Zero-Field Nucleation and Fast Motion of Skyrmions Induced by Nanosecond Current Pulses in a Ferrimagnetic Thin Film

Yassine Quessab,* Jun-Wen Xu, Egecan Cogulu, Simone Finizio, Jörg Raabe, and Andrew D. Kent*



Cite This: *Nano Lett.* 2022, 22, 6091–6097



Read Online

ACCESS |

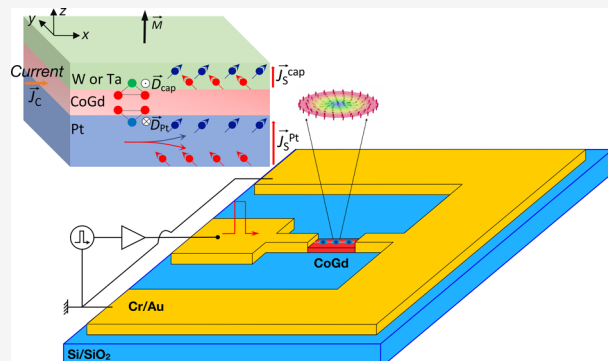
Metrics & More

Article Recommendations

Supporting Information

ABSTRACT: Skyrmion racetrack memories are highly attractive for next-generation data storage technologies. Skyrmions are noncollinear spin textures stabilized by chiral interactions. To achieve a fast-operating memory device, it is critical to move skyrmions at high speeds. The skyrmion dynamics induced by spin-orbit torques (SOTs) in the commonly studied ferromagnetic films is hindered by strong pinning effects and a large skyrmion Hall effect causing deflection of the skyrmion toward the racetrack edge, which can lead to information loss. Here, we investigate the current-induced nucleation and motion of skyrmions in ferrimagnetic Pt/CoGd/(W or Ta) thin films. We first reveal field-free skyrmion nucleation mediated by Joule heating. We then achieve fast skyrmion motion driven by SOTs with velocities as high as 610 m s^{-1} and a small skyrmion Hall angle $|\theta_{\text{SkHE}}| \lesssim 3^\circ$. Our results show that ferrimagnets are better candidates for fast skyrmion-based memory devices with low risk of information loss.

KEYWORDS: magnetic skyrmions, domain walls, spin-orbit torques, current-induced motion, magnetization dynamics



The development of efficient artificial intelligence technologies highly depends on the resolution of a memory bottleneck, that is, to achieve high memory bandwidth and low latency. Magnetic memories, such as skyrmion-based racetrack memories, are a promising candidate for a fast encoding of bits. Magnetic skyrmions as information carriers have been investigated for a wide range of applications such as nonvolatile memory, logic, and computing devices.^{1–4} Skyrmions are quasiparticles that offer the advantage of topological protection for data retention, and they can be manipulated by spin-orbit torques (SOTs) using current pulses.^{5–9} Small skyrmions have been observed at room temperature in ultrathin films.^{10,11} Yet, a key challenge that remains to be addressed for racetrack memory applications is to move them at high speeds. Several studies have reported skyrmion motion induced by SOTs with velocities of up to 100 m s^{-1} in ultrathin ferromagnetic films.^{5,6,8,12,13} However, in these materials the large dipolar interactions, strong pinning, and Walker breakdown^{14,15} are considerable obstacles to achieve efficient and fast skyrmion motion. In addition, the skyrmion dynamics in ferrimagnets is highly impacted by the skyrmion Hall effect (SkHE), that is, a transverse displacement with regards to the current flow direction as result of the Magnus force that arises from the nonzero topological charge.^{5,8,9} The transverse deflection is characterized by the so-called skyrmion Hall angle (θ_{SkHE}). It is desirable to minimize the SkHE as it can lead to skyrmion annihilation at the edge of a racetrack.

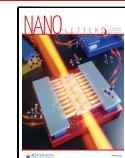
On the other hand, nearly compensated ferrimagnetic materials are an attractive alternative due to their weak dipolar fields and fast spin dynamics which led to the prediction of smaller and faster skyrmions.^{14,16} Skyrmions as small as 10 nm have been observed in a ferrimagnetic CoGd thin film but their current-induced motion was not studied.¹¹ Ferrimagnetic alloys benefit from angular momentum compensation that can suppress the Walker breakdown and reduce pinning effects, therefore allowing a fast spin dynamics. As a result, current-induced domain wall (DW) motion with velocities of up to 1300 m s^{-1} has been observed in CoGd films at the angular momentum compensation temperature.¹¹ In contrast, skyrmion motion with a velocity of only 50 m s^{-1} has been reported in a ferrimagnetic multilayer.⁷ Hence, the fast motion of skyrmions induced by SOTs predicted in ferrimagnets remains thus far elusive.

In this article, we investigate the formation and manipulation of skyrmions using ultrashort current pulses by magneto-optical Kerr effect (MOKE) and scanning transmission X-ray microscopy (STXM) at room temperature in ferrimagnetic

Received: March 15, 2022

Revised: July 15, 2022

Published: July 25, 2022



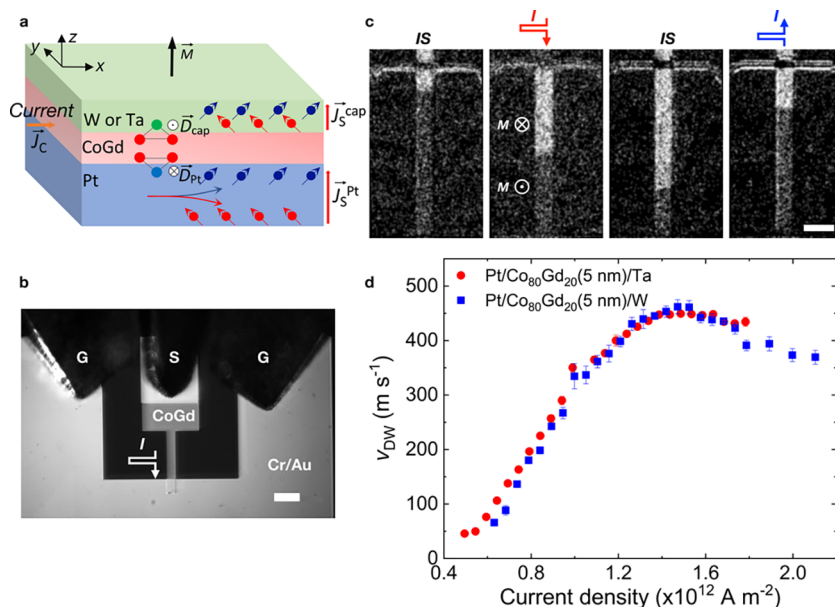


Figure 1. Current-induced domain wall dynamics. (a) Schematic representation of the studied films where the bottom Pt and capping (W or Ta) layers both contribute to the DMI (\vec{D}_{Pt} and \vec{D}_{cap}) and spin currents ($\vec{j}_{\text{S}}^{\text{Pt}}$ and $\vec{j}_{\text{S}}^{\text{cap}}$) that are associated with the spin Hall-effect from the injection of a charge current (j_{C}). (b) Optical image of the device studied for DW dynamics induced by SOTs. An amplified 5 ns current pulse is injected into the device through a ground-signal-ground (GSG) probe. The scale bar is 30 μm . (c) Differential MOKE images taken in the initial state (IS) and after applying positive (red) or negative (blue) current pulses. The scale bar is 20 μm . (d) DW velocity (v_{DW}) measured as a function of the heavy metal current density (Methods) in Pt/CoGd/(W or Ta) films.

CoGd thin films. We demonstrate zero field current-induced nucleation of skyrmions and fast motion driven by SOTs with velocities of up to 610 m s⁻¹. Direct observation of the SkHE confirms that the spin textures have a nontrivial topology and are therefore skyrmions. We report a skyrmion Hall angle (θ_{SkHE}) of less than 3°, much smaller than in ferromagnets. We also show evidence that the skyrmion nucleation is a thermal process. Our results provide a path forward for a fast encoding and storage of data using skyrmion-based racetrack memory devices.

Here, our goal is to achieve fast current-induced skyrmion dynamics at room temperature, and for this purpose we studied nearly compensated ferrimagnetic thin films, Pt(6 nm)/Co₈₀Gd₂₀(5 nm)/(W or Ta)(3 nm), that were grown by DC magnetron sputtering and deposited onto a Si/SiO₂ or SiN substrate for MOKE and X-ray microscopy, respectively (see Methods in Supporting Information). The ferrimagnetic films were patterned into μm -wide racetracks to study the current-induced DW and skyrmion motion.

In previous studies, we optimized the growth of CoGd thin films and carried out a systematic study of the Dzyaloshinskii-Moriya interactions (DMI)^{17,18} and SOTs¹⁹ as a function of the capping layer. The CoGd structures were designed to have large perpendicular magnetic anisotropy and a fully saturated state at remanence^{17,19} to allow the nucleation of isolated metastable skyrmions. The alloy composition was chosen to yield magnetic and angular momentum compensation close to room temperature with $T_{\text{M}} = 250$ K for both CoGd films and $T_{\text{A}} = 285$ and 292 K for Pt/CoGd/Ta and Pt/CoGd/W, respectively, where T_{M} and T_{A} denotes the magnetic and angular momentum compensation temperature, respectively.¹⁹ Minimization of the angular momentum at room temperature in our CoGd thin films indicates the potential of fast current-induced dynamics.^{11,20,21} As seen in Figure 1a, the CoGd layer is inserted between two heavy metals which both contribute to

the DMI and generation of spin currents. W and Ta capping were chosen to optimize the SOTs due to their giant negative spin-Hall angle (SHA)^{22–24} as opposed to commonly studied Pt/ferro- or ferri-magnet/oxide structures.^{7,8,11} We measured a maximum effective SHA of 16.5% and 6.5% for Pt/CoGd/W and Pt/CoGd/Ta, respectively.¹⁹

We first investigated the DW motion induced by 5 ns current pulses by MOKE microscopy in a 10 μm wide racetrack, as shown in Figure 1b. A DW is initially nucleated by applying a current pulse in the presence of a small out-of-plane magnetic field. In Figure 1c, we show a sequence of differential MOKE images before and after injecting a train of current pulses at zero magnetic field. Changing the current polarity reverses the DW displacement. In addition, up-to-down and down-to-up DWs move in the same direction along the current flow consistent with SOTs-driven motion of Néel DWs.^{25,26} Figure 1d summarizes the DW velocity (v_{DW}) as a function of the current density (j) for Pt/CoGd (W or Ta) thin films. We measured a maximum DW velocity of $v_{\text{DW}} = 448$ and 460 m s⁻¹ for Pt/CoGd/Ta and Pt/CoGd/W, respectively. In the flow regime, we measured a DW mobility of $\mu_{\text{DW}} = 608$ and 657 m s⁻¹/(10¹² A m⁻²), and a depinning current density threshold of $j_{\text{dep}} = 0.47$ and 0.52×10^{12} A m⁻² for CoGd films capped by Ta and W, respectively. Saturation of the DW velocity is observed for $j > 1.3 \times 10^{12}$ A m⁻². The current-induced DW motion can be described by the one-dimensional (1D) model^{27,28} modified for ferrimagnets as described by Caretta et al.¹¹ The saturation regime depends only on the DMI and the spin density, that is, angular momentum. The fast DW velocities we report are thus consistent with the angular momentum compensation that is close to room temperature in our CoGd thin films. At large current densities, $j > 1.6 \times 10^{12}$ A m⁻², we observed a decrease in the DW velocity. We attribute this to heating effects in the CoGd films that results in an increase of the net angular momentum and thus a decrease

of the DW velocity ([Supporting Information](#)). Additionally, the Joule heating is also responsible for the lower DW velocities compared to recent studies that reported DW velocities higher than 1000 m s^{-1} in CoGd-based ferrimagnets^{11,29} as the heating pushes our CoGd films away from angular momentum compensation. These results demonstrate that the CoGd films we optimized^{17,19} have low DW pinning and density of natural defects leading to fast DW motion induced by SOTs making these structures ideal to study skyrmion motion.

Here, we examined the current-induced nucleation of skyrmions in Pt/CoGd/(W or Ta) thin films by MOKE microscopy in a device similar to [Figure 1b](#) (see Methods in [Supporting Information](#)). The samples are initially saturated and uniformly magnetized either in the up ([Figure 2a,c](#)) or

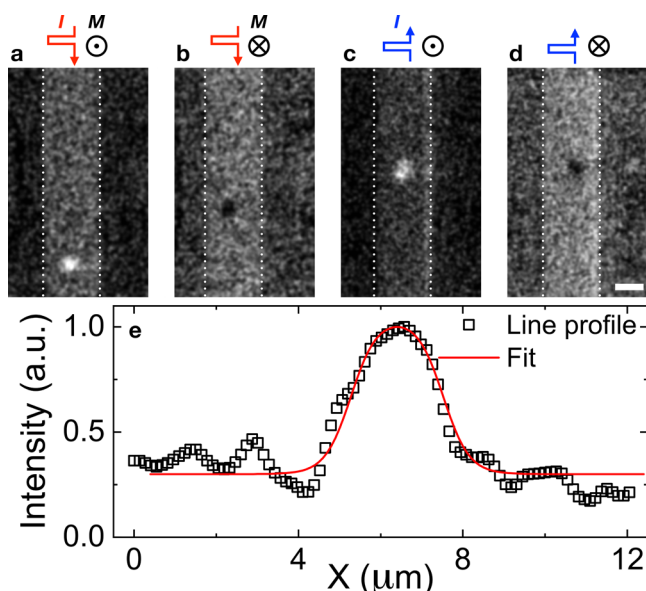


Figure 2. Current-induced skyrmion nucleation. (a–d) Differential MOKE images taken after injecting a single 5 ns current pulse at zero magnetic field with a positive (a,b) or negative (c,d) polarity in Pt/CoGd/Ta (for Pt/CoGd/W, see [Supporting Information](#)). The CoGd magnetization is initially set in the up (a,c) or down (b,d) direction. A current density of $j = 1.81 \times 10^{12} \text{ A m}^{-2}$ is used for the nucleation. Panel e shows an intensity plot of the skyrmion nucleated in panel a fitted with a 360° Néel DW model convoluted with a Gaussian beam and a DW width of about 20 nm (see [Supporting Information](#) in refs 10 and 30). A skyrmion diameter of $\sim 1.20 \mu\text{m}$ is found. The dotted lines indicate the boundaries of the racetrack. The scale bar is $5 \mu\text{m}$.

down ([Figure 2b,d](#)) direction. Skyrmion nucleation is achieved after applying a single 5 ns current pulse with either a positive (red) or negative (blue) polarity as shown in the differential MOKE images in [Figure 2a–d](#). Circular regions of contrast opposite to the background correspond to the skyrmions. A bright (dark) MOKE contrast indicate a skyrmion with a core pointing down (up). Isolated skyrmions are nucleated in our CoGd films at zero magnetic field and from a uniformly magnetized state. In contrast, most studies in the literature employ an external out-of-plane magnetic field to nucleate and stabilize skyrmions from a wormlike domain state.^{3,5,7,9,11,31} A profile line scan of the skyrmion in [Figure 2a](#) is shown in [Figure 2e](#) and fitted with a 360° DW model. We found a skyrmion diameter of about $\sim 1.20 \mu\text{m}$. We experimentally

determined a nucleation current density threshold of 1.81 and $1.90 \times 10^{12} \text{ A m}^{-2}$ for CoGd films capped by Ta and W, respectively. As seen in [Figures 2a–d](#), an isolated skyrmion is nucleated regardless of the initial magnetization direction and the current polarity. Consequently, we can rule out a nucleation induced by SOTs³² or Oersted fields.¹³ Instead, our experimental results indicate that the skyrmion nucleation is a thermal process. This is in agreement with the recent demonstrations of thermal generation of skyrmions by a femtosecond laser heat pulse^{33,34} or on chip electrical heaters.³⁵

We then studied the manipulation of skyrmions by SOTs using MOKE microscopy (see Methods in [Supporting Information](#)). Skyrmions are nucleated at zero magnetic field as previously discussed ([Figure 3a–i,b–i](#)) then a small out-of-plane magnetic field $\mu_0 H_z = -10 \text{ mT}$ is applied to stabilize the core of the skyrmion. In [Figure 3a,b](#), we show a sequence of differential MOKE images after applying a single 5 ns current pulse with a positive ([Figure 3a,ii–vi](#)) or negative ([Figures 3b,ii–vi](#)) polarity for the Pt/CoGd/Ta film. A current density (see Methods in [Supporting Information](#)) of $j = 1.5 \times 10^{12}$ and $1.8 \times 10^{12} \text{ A m}^{-2}$ is used in [Figure 3a,b](#), respectively. The skyrmion with a core pointing down moves downward upon injection of a positive current pulse and by reversing the current polarity the skyrmion moves upward. Skyrmions with a core pointing up or down both are displaced in the same direction, along the current flow, indicating that, indeed, the skyrmion motion is driven by SOTs ([Supporting Information](#)). In [Figure 3a](#), after the third current pulse, the upper skyrmion collapsed. This stochastic annihilation may be attributed to thermal instability due to the temperature increase induced by the current pulse ([Supporting Information](#)). In [Figure 3c](#), we summarize the skyrmion velocity measured in Pt/CoGd/(W or Ta) films. We found a maximum skyrmion velocity (v_{SK}) of 610 and 500 m s^{-1} for the CoGd films capped by W and Ta, respectively. These are the highest skyrmion velocities reported thus far in the literature.^{6–9}

The flow regime, for which the skyrmion velocity linearly increases with the current density, can be observed for $0.8 < j < 1.1 (\times 10^{12} \text{ A m}^{-2})$ in Pt/CoGd/W and $0.75 < j < 1.2 (\times 10^{12} \text{ A m}^{-2})$ in Pt/CoGd/Ta. In this regime, we find a skyrmion mobility $\mu_{SK} = 920$ and $608 \text{ m s}^{-1}/(10^{12} \text{ A m}^{-2})$, and a depinning current density threshold of $j_{dep} = 0.45$ and $0.39 \times 10^{12} \text{ A m}^{-2}$ for CoGd films capped by W and Ta, respectively. On the basis of the Thiele equation, it is expected that the skyrmion velocity scales linearly with the current density with $v_{SK} = \mu_{SK} j$.³⁶ However, we observed a saturation regime. This deviation from the Thiele equation, which considers the skyrmion as a rigid texture, has been explained by the deformation of the skyrmion when it is displaced at high speeds in the flow regime.^{4,5,9} Yet, the saturation regime is short-lived as we observed a decrease of the skyrmion velocity at larger current densities for $j > 1.4 \times 10^{12} \text{ A m}^{-2}$ and $j > 1.5 \times 10^{12} \text{ A m}^{-2}$ for CoGd films capped by W and Ta, respectively ([Figure 3c](#)). This behavior is similar to the current-induced DW dynamics as previously discussed, which can be explained by heating effects ([Supporting Information](#)).

The skyrmion velocity reported as higher in Pt/CoGd/W than in Pt/CoGd/Ta films is a result of a larger DMI and smaller angular momentum based on our previous studies.^{17–19} For both CoGd films, the skyrmions move faster than DWs ([Figures 1d](#) and [3c](#)). According to the Thiele model, the linearity of the skyrmion velocity with the current density^{4,14,36}

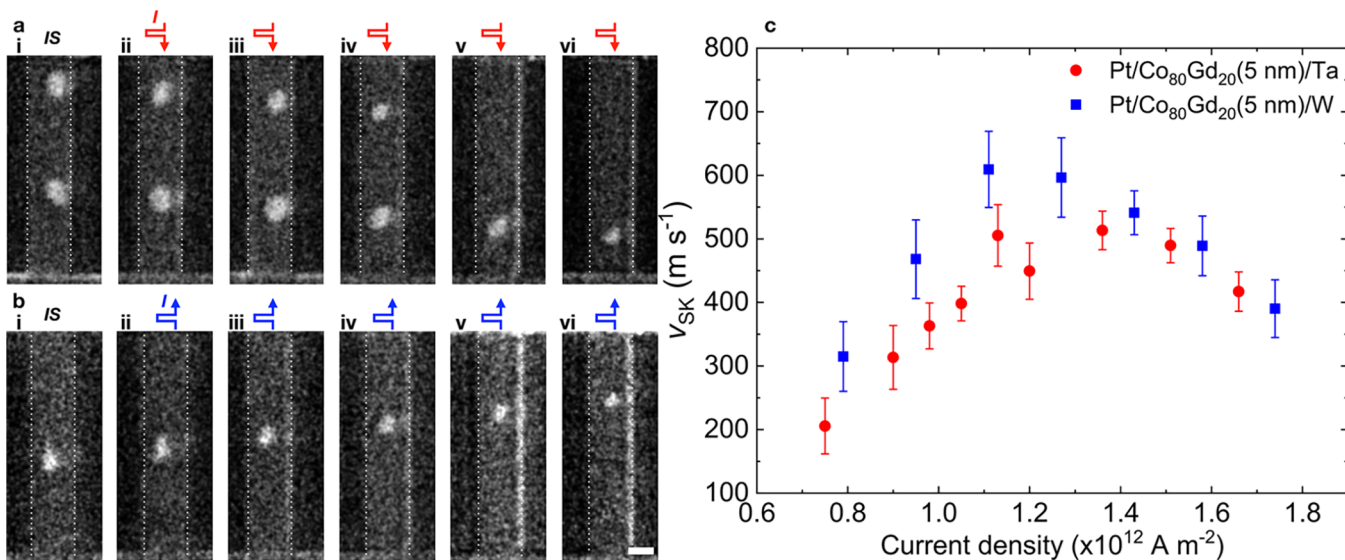


Figure 3. Current-induced skyrmion dynamics. (a,b) Sequence of differential MOKE images showing the SOT-driven skyrmion motion in Pt/CoGd/Ta induced by a single positive (a(ii–vi)) and negative (b(ii–vi)) current pulse with a current density of $j = 1.5 \times 10^{12}$ and $1.8 \times 10^{12} \text{ A m}^{-2}$, respectively. A skyrmion is initially nucleated at zero magnetic field (a-i and b-i). $\mu_0 H_z = -10 \text{ mT}$ is applied to stabilize the skyrmion in a(ii–vi) and b(ii–vi). (c) Summary of the measured skyrmion velocity (v_{SK}) for CoGd films capped by W and Ta. The scale bar is $5 \mu\text{m}$.

suggests that the SOT-driven skyrmion motion could surpass DWs that are described by the 1D model^{11,27,28} as long as the skyrmion remains rigid.

By tracking the (X, Y) coordinates of the skyrmion (see Methods in Supporting Information), we can monitor the position of the skyrmions along the racetrack after injecting a ns current pulse. The coordinates of three skyrmions are shown in Figure 4e after applying a single current pulse with a density $j = 1.51 \times 10^{12} \text{ A m}^{-2}$. The first data point for each skyrmion indicates the initial position after nucleation. A transverse deflection with regards to the x -axis can be observed as the skyrmion is displaced, which is indicative of the SkHE.^{5,36,37} As depicted in the inset in Figure 4e, the skyrmion velocity (\vec{v}) acquires a y -component due to the Magnus force (\vec{F}_M). The skyrmion Hall angle (SkHA, θ_{SkHE}) quantifies the deflection with regards to the current flow direction.

Figure 4a–d shows the initial and final position of a skyrmion after injecting a series of positive (Figures 4a,b) and negative (Figure 4c,d) current pulses, respectively. By superimposing the initial and final state, we can observe that the skyrmion moves downward and to the left (Figure 4a,b) for a positive current pulse and upward and to the right for a negative current pulse (Figure 4c,d). Therefore, the deflection angle (with respect to the skyrmion motion) remains unchanged upon reversal of the current polarity which confirms that the transverse skyrmion motion indeed arises from the SkHE. In addition, the Magnus force is a direct consequence of a nonzero topological charge $Q = \pm 1$. Therefore, we can confirm that the spin textures we observed by MOKE microscopy are topological and, hence, are skyrmions.

In Figure 4f, the SkHA is plotted as a function of the skyrmion velocity and capping layer. Both CoGd films exhibit a very similar behavior with a very low SkHA $|\theta_{\text{SkHE}}| \lesssim 3^\circ$. The SkHA remains fairly insensitive to the skyrmion velocity despite the large speeds reported. In contrast, in ferromagnetic materials^{5,8,9} and ferrimagnetic multilayers,⁷ a significant current drive dependence of the SkHA was found, which was

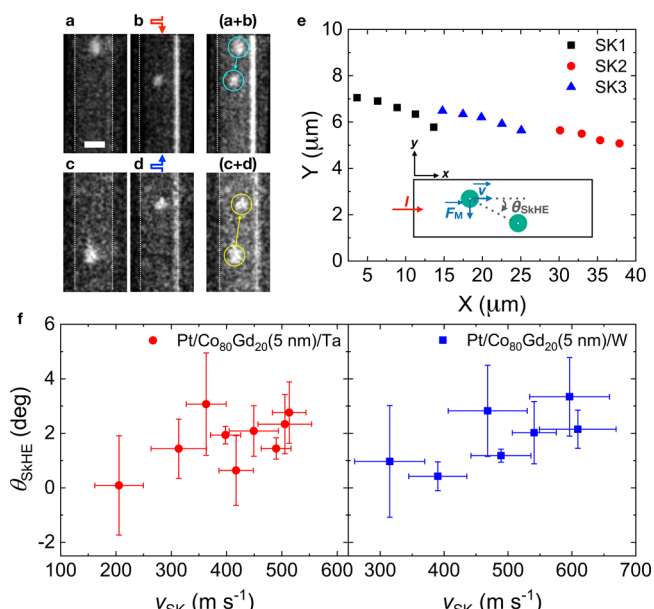


Figure 4. Topology signature of the skyrmions. (a,c) A skyrmion initially nucleated at zero field in Pt/CoGd/Ta then after injection of (b) $N = 4$ and (d) $N = 5$ pulses with a current density $j = \pm 1.51 \times 10^{12} \text{ A m}^{-2}$. (e) Tracking of three skyrmions coordinates after applying a single 5 ns current pulse as in panels a and b. Inset shows the SkHE and the transverse displacement of the skyrmion with respect to the current flow direction. (f) Summary of the skyrmion Hall angle ($|\theta_{\text{SkHE}}|$) measured in CoGd films capped by W and Ta as a function of the skyrmion velocity measured in Figure 3c. The scale bar is $5 \mu\text{m}$.

explained by the presence of strong pinning sites and film disorder. Therefore, our results indicate that skyrmions are more rigid in our CoGd films due to a lower level of disorder. Indeed, during the skyrmion motion experiment, no deformation was observed as seen in Figure 3a,b as opposed to the strong deformation of skyrmions observed in ferromagnets.^{5,8,9} This higher skyrmion rigidity in our CoGd

films may be responsible for the higher skyrmion velocities reported here.

In addition, the SkHA $|\theta_{\text{SkHE}}| \lesssim 3^\circ$ measured in our CoGd films is much smaller than in ferromagnetic materials such as Pt/Co/MgO ($|\theta_{\text{SkHE}}| \simeq 50^\circ$)⁸ and Pt/CoFeB/MgO multilayer ($|\theta_{\text{SkHE}}| \simeq 30^\circ$)^{3,9} even though the reported maximum velocities ($\sim 100 \text{ m s}^{-1}$) are also smaller than in our CoGd films. Even for a skyrmion of a similar size than in this study (in the μm scale), in a ferromagnet-based synthetic antiferromagnet the authors reported a SkHA of $|\theta_{\text{SkHE}}| \simeq 20^\circ$ for a maximum velocity 2 orders of magnitude smaller.³⁸ Our results can be explained by the fact that the studied CoGd films have an angular momentum compensation close to room temperature and therefore a small net spin density of $S = 7.4 \times 10^{-8}$ and $1.5 \times 10^{-8} \text{ J s m}^{-3}$ for CoGd films capped by Ta and W, respectively (Supporting Information), that is about 2 orders of magnitude smaller than the spin density of a Co ferromagnetic thin film. This is consistent with a recent study that showed a vanishing SkHA in a single ferrimagnetic layer at the angular momentum compensation point.³⁹

We also investigated the current-induced skyrmion nucleation by X-ray microscopy in the same CoGd films (see Methods in Supporting Information) as represented in Figure 5a. An X-ray magnetic circular dichroism (XMCD) image is taken after applying the 5 ns current pulses at zero magnetic field. The Pt/CoGd/W film is initially saturated in the up- and down- direction in Figure 5b,d, respectively. $N = 100$ pulses with a current density of $j = 8.6 \times 10^{11} \text{ A m}^{-2}$ resulted in the nucleation of a skyrmion with a core pointing down (Figure 5b) or up (Figure 5d). A close-up XMCD image of the skyrmion is shown in Figure 5c,e. A scan profile of the skyrmion (encircled by the dotted line) is displayed in Figure 5f. We measured a skyrmion diameter of $\sim 100 \text{ nm}$ much smaller than the skyrmions observed in the same film by MOKE. Additionally, the 100 nm skyrmions had a longer lifetime (at least 12 h) while the larger skyrmions at zero magnetic field were stable only for a few minutes. This indicates that these two types of skyrmions are associated with a different energy barrier. This is consistent with magnetic films with a moderate DMI parameter for which the DMI and dipolar interactions compete which can lead to several skyrmion energy minima resulting in various sizes and lifetimes.¹⁴ As a result, the smaller 100 nm skyrmions are the most favorable and stable in our CoGd films.

The skyrmion diameter is determined by the saturation magnetization, magnetic anisotropy, DMI and magnetic thickness among other parameters.^{4,14,16} Despite the low saturation magnetization of our CoGd films, the smallest skyrmion diameter achieved is of similar magnitude than in ferromagnets.^{8,9} By capping the CoGd layer with a heavy metal such as W and Ta, the SOTs are enhanced. However, this results in a smaller net DMI energy of $\sim 0.23 \text{ mJ m}^{-2}$ ^{17–19} compared to $> 1 \text{ mJ m}^{-2}$ in Pt/ferromagnet/oxide materials.^{8–10} In addition, the magnetic layer is thinner in our study than the 12 nm CoGd films investigated by Caretta et al.¹¹ Our results are consistent with the full stray field model developed by Büttner et al. which shows that at low-to-moderate DMI values smaller skyrmions can be achieved in thicker films.¹⁴

In conclusion, we have demonstrated field-free nucleation of bubble skyrmions and 100 nm skyrmions induced by nanosecond current pulses in ferrimagnetic CoGd thin films. We provided evidence that the skyrmion nucleation is a

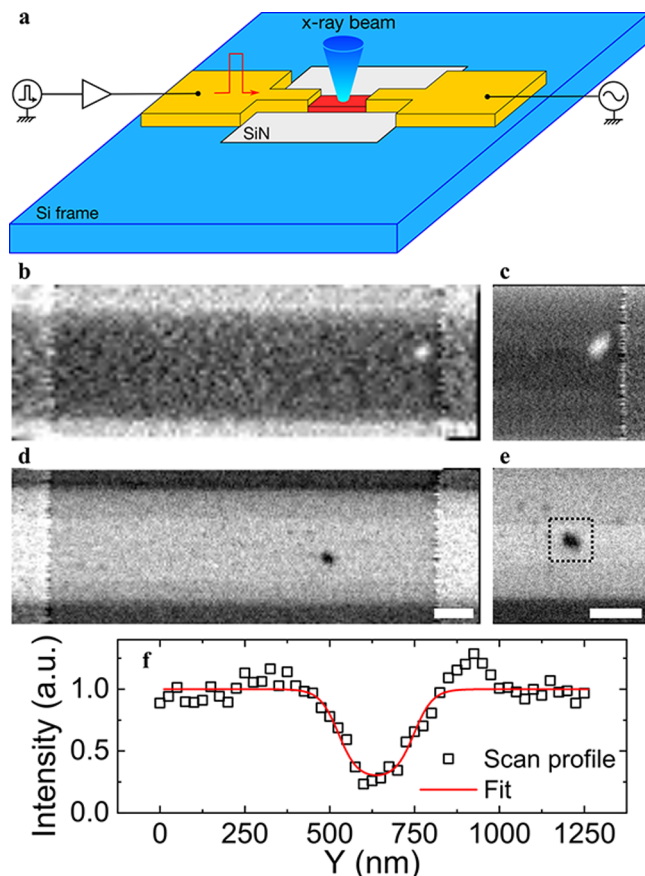


Figure 5. Small skyrmions imaged by STXM. (a) Schematic representation of the X-ray experiment. A circularly polarized X-ray beam is focused onto the CoGd wire deposited onto a SiN membrane. An amplified 5 ns current pulse is injected into the wire through Cr/Au contact pads, and the device is terminated by an oscilloscope. (b,d) A train of $N = 100$ current pulses is used to nucleate a skyrmion at zero field with a current density $j = 8.6 \times 10^{11} \text{ A m}^{-2}$ in Pt/CoGd/W. The sample is initially saturated in the (b) up or (d) down direction. (c,e) Higher resolution scan of the region where the skyrmion is nucleated. (f) Intensity scan profile of the skyrmion shown in panel e. A skyrmion diameter of $\sim 100 \text{ nm}$ is found. The scale bar is $1 \mu\text{m}$.

thermal process. We have also demonstrated fast skyrmion motion driven by SOTs with velocities as high as 610 m s^{-1} in CoGd structures that were optimized for large SOTs, low saturation magnetization and spin density at room temperature. We showed that spin textures with topology move faster than domain walls. The current-induced dynamics of DWs and skyrmions is less impacted by disorder in CoGd compared to ferromagnets. We measured a small SkHA of $|\theta_{\text{SkHE}}| \lesssim 3^\circ$ at large skyrmion velocities. We proved that fast skyrmion motion with minimal transverse deflection can be achieved in a nearly compensated ferrimagnets with low spin density. The fast skyrmion motion we reported in ferrimagnets could allow magnetic memories to operate at higher gigahertz regimes. Therefore, our experimental results demonstrate that ferrimagnets are a better platform than ferromagnets to implement a skyrmion-based racetrack memory device for technologies requiring faster encoding and storage of information. Beyond memory applications, our findings also pave the way for fast new computing technologies based on skyrmions using ferrimagnetic materials.⁴

■ ASSOCIATED CONTENT

SI Supporting Information

The Supporting Information is available free of charge at <https://pubs.acs.org/doi/10.1021/acs.nanolett.2c01038>.

Detailed methods section about the film deposition, MOKE and X-ray microscopy, current pulse parameters, and skyrmion velocity and Hall angle measurements; additional experimental information about the current-induced domain wall motion; additional experimental images for the current-induced skyrmion nucleation and motion in Pt/CoGd/(W or Ta) thin films; discussion about the heating effects on the domain wall and skyrmion dynamics; calculation of the temperature increase in the devices used for the domain wall and skyrmion measurements ([PDF](#))

■ AUTHOR INFORMATION

Corresponding Authors

Yassine Quessab — *Center for Quantum Phenomena, Department of Physics, New York University, New York, New York 10003, United States;*  orcid.org/0000-0003-0199-6025; Email: yassine.quessab@nyu.edu

Andrew D. Kent — *Center for Quantum Phenomena, Department of Physics, New York University, New York, New York 10003, United States;*  orcid.org/0000-0002-9050-8822; Email: andy.kent@nyu.edu

Authors

Jun-Wen Xu — *Center for Quantum Phenomena, Department of Physics, New York University, New York, New York 10003, United States*

Egecan Cogulu — *Center for Quantum Phenomena, Department of Physics, New York University, New York, New York 10003, United States;*  orcid.org/0000-0001-5568-3476

Simone Finizio — *Swiss Light Source, Paul Scherrer Institut, 5232 Villigen PSI, Switzerland;*  orcid.org/0000-0002-1792-0626

Jörg Raabe — *Swiss Light Source, Paul Scherrer Institut, 5232 Villigen PSI, Switzerland;*  orcid.org/0000-0002-2071-6896

Complete contact information is available at:
<https://pubs.acs.org/10.1021/acs.nanolett.2c01038>

Author Contributions

A.D.K. and Y.Q. proposed the study. Y.Q. conceived and planned the experiments. Y.Q. grew, optimized, and characterized the CoGd films. Y.Q. designed and built the MOKE microscope and performed the DW and skyrmion experiments. Y.Q. and S.F. carried out the X-ray microscopy measurements under the supervision of J.R. J.-W.X. and Y.Q. did the lithography fabrication of the devices. E.C. performed the COMSOL multiphysics simulations. All of the authors participated in the discussion and interpretation of the experimental results. Y.Q. and A.D.K. drafted the manuscript, and all of the authors contributed to and commented on it.

Notes

The authors declare no competing financial interest.

■ ACKNOWLEDGMENTS

This work was supported by the DARPA Grant D18AP00009. The studied devices were patterned at the Advanced Science

Research Center NanoFabrication Facility of the Graduate Center at the City University of New York. Part of this work was performed at the PolLux (X07DA) beamline of the Swiss Light Source, Paul Scherrer Institut, Villigen PSI, Switzerland. The PolLux endstation was financed by the German Bundesministerium für Bildung und Forschung through contracts 05K16WED and 05K19WE2.

■ REFERENCES

- (1) Fert, A.; Cros, V.; Sampaio, J. Skyrmions on the track. *Nat. Nanotechnol.* **2013**, *8*, 152.
- (2) Zhang, X.; Ezawa, M.; Zhou, Y. Magnetic skyrmion logic gates: conversion, duplication and merging of skyrmions. *Sci. Rep.* **2015**, *5*, 9400.
- (3) Song, K. M.; Jeong, J.-S.; Pan, B.; Zhang, X.; Xia, J.; Cha, S.; Park, T.-E.; Kim, K.; Finizio, S.; Raabe, J.; Chang, J.; Zhou, Y.; Zhao, W.; Kang, W.; Ju, H.; Woo, S. Skyrmion-based artificial synapses for neuromorphic computing. *Nature Electronics* **2020**, *3*, 148–155.
- (4) Vakili, H.; Xu, J.-W.; Zhou, W.; Sakib, M. N.; Morshed, M. G.; Hartnett, T.; Quessab, Y.; Litzius, K.; Ma, C. T.; Ganguly, S.; Stan, M. R.; Balachandran, P. V.; Beach, G. S. D.; Poon, S. J.; Kent, A. D.; Ghosh, A. W. Skyrmionics—computing and memory technologies based on topological excitations in magnets. *J. Appl. Phys.* **2021**, *130*, 070908.
- (5) Litzius, K.; Lemesh, I.; Kruger, B.; Bassirian, P.; Caretta, L.; Richter, K.; Buttner, F.; Sato, K.; Tretiakov, O. A.; Forster, J.; Reeve, R. M.; Weigand, M.; Bykova, I.; Stoll, H.; Schutz, G.; Beach, G. S. D.; Klau, M. Skyrmion Hall effect revealed by direct time-resolved x-ray microscopy. *Nat. Phys.* **2017**, *13*, 170–175.
- (6) Legrand, W.; Maccariello, D.; Reyren, N.; Garcia, K.; Moutafis, C.; Moreau-Luchaire, C.; Collin, S.; Bouzehouane, K.; Cros, V.; Fert, A. Room-temperature current-induced generation and motion of sub-100 nm skyrmions. *Nano Lett.* **2017**, *17*, 2703–2712.
- (7) Woo, S.; Song, K. M.; Zhang, X.; Zhou, Y.; Ezawa, M.; Liu, X.; Finizio, S.; Raabe, J.; Lee, N. J.; Kim, S.-I.; Park, S.-Y.; Kim, Y.; Kim, J.-Y.; Lee, D.; Lee, O.; Choi, J. W.; Min, B.-C.; Koo, H. C.; Chang, J. Current-driven dynamics and inhibition of the skyrmion Hall effect of ferrimagnetic skyrmions in gdfeo films. *Nat. Commun.* **2018**, *9*, 959.
- (8) Juge, R.; Je, S.-G.; Chaves, D. d. S.; Buda-Prejbeanu, L. D.; Pen-Garcia, J.; Nath, J.; Miron, I. M.; Rana, K. G.; Aballe, L.; Foerster, M.; Genuzio, F.; Mentes, T. O.; Locatelli, A.; Maccherozzi, F.; Dhesi, S. S.; Belmeguenai, M.; Roussigne, Y.; Auffret, S.; Pizzini, S.; Gaudin, G.; Vogel, J.; Boulle, O. Current-driven skyrmion dynamics and drive-dependent skyrmion Hall effect in an ultrathin film. *Physical Review Applied* **2019**, *12*, 044007.
- (9) Litzius, K.; Leliaert, J.; Bassirian, P.; Rodrigues, D.; Kromin, S.; Lemesh, I.; Zazvorka, J.; Lee, K.-J.; Mulders, J.; Kerber, N.; Heinze, D.; Keil, N.; Reeve, R. M.; Weigand, M.; Van Waeyenberge, B.; Schutz, G.; Everschor-Sitte, K.; Beach, G. S. D.; Klau, M. The role of temperature and drive current in skyrmion dynamics. *Nature Electronics* **2020**, *3*, 30–36.
- (10) Boulle, O.; Vogel, J.; Yang, H.; Pizzini, S.; de Souza Chaves, D.; Locatelli, A.; Mentes, T. O.; Sala, A.; Buda-Prejbeanu, L. D.; Klein, O.; Belmeguenai, M.; Roussigne, Y.; Stashkevich, A.; Cherif, S. M.; Aballe, L.; Foerster, M.; Chshiev, M.; Auffret, S.; Miron, I. M.; Gaudin, G. Room-temperature chiral magnetic skyrmions in ultrathin magnetic nanostructures. *Nat. Nanotechnol.* **2016**, *11*, 449–454.
- (11) Caretta, L.; Mann, M.; Buttner, F.; Ueda, K.; Pfau, B.; Gunther, C. M.; Helsing, P.; Churikova, A.; Klose, C.; Schneider, M.; Engel, D.; Marcus, C.; Bono, D.; Bagschik, K.; Eisebitt, S.; Beach, G. S. D. Fast current-driven domain walls and small skyrmions in a compensated ferrimagnet. *Nat. Nanotechnol.* **2018**, *13*, 1154–1160.
- (12) Hrabec, A.; Sampaio, J.; Belmeguenai, M.; Gross, I.; Weil, R.; Chérif, S. M.; Stashkevich, A.; Jacques, V.; Thiaville, A.; Rohart, S. Current-induced skyrmion generation and dynamics in symmetric bilayers. *Nat. Commun.* **2017**, *8*, 15765.
- (13) Woo, S.; Litzius, K.; Kruger, B.; Im, M.-Y.; Caretta, L.; Richter, K.; Mann, M.; Krone, A.; Reeve, R. M.; Weigand, M.; Agrawal, P.;

- Lemesh, I.; Mawass, M.-A.; Fischer, P.; Klaui, M.; Beach, G. S. D. Observation of room-temperature magnetic skyrmions and their current-driven dynamics in ultrathin metallic ferromagnets. *Nat. Mater.* **2016**, *15*, 501.
- (14) Buttner, F.; Lemesh, I.; Beach, G. S. D. Theory of isolated magnetic skyrmions: From fundamentals to room temperature applications. *Sci. Rep.* **2018**, *8*, 4464.
- (15) Lemesh, I.; Beach, G. S. D. Walker breakdown with a twist: Dynamics of multilayer domain walls and skyrmions driven by spin-orbit torque. *Physical Review Applied* **2019**, *12*, 044031.
- (16) Ma, C. T.; Xie, Y.; Sheng, H.; Ghosh, A. W.; Poon, S. J. Robust formation of ultrasmall room-temperature Néel skyrmions in amorphous ferrimagnets from atomistic simulations. *Sci. Rep.* **2019**, *9*, 9964.
- (17) Quessab, Y.; Xu, J.-W.; Ma, C. T.; Zhou, W.; Riley, G. A.; Shaw, J. M.; Nembeh, H. T.; Poon, S. J.; Kent, A. D. Tuning interfacial Dzyaloshinskii-Moriya interactions in thin amorphous ferrimagnetic alloys. *Sci. Rep.* **2020**, *10*, 7447.
- (18) Morshed, M. G.; Khoo, K. H.; Quessab, Y.; Xu, J.-W.; Laskowski, R.; Balachandran, P. V.; Kent, A. D.; Ghosh, A. W. Tuning Dzyaloshinskii-Moriya interaction in ferrimagnetic GdCo: A first-principles approach. *Phys. Rev. B* **2021**, *103*, 174414.
- (19) Quessab, Y.; Xu, J.-W.; Morshed, M. G.; Ghosh, A. W.; Kent, A. D. Interplay between spin-orbit torques and Dzyaloshinskii-Moriya interactions in ferrimagnetic amorphous alloys. *Advanced Science* **2021**, *8*, 2100481.
- (20) Kim, K.-J.; Kim, S. K.; Hirata, Y.; Oh, S.-H.; Tono, T.; Kim, D.-H.; Okuno, T.; Ham, W. S.; Kim, S.; Go, G.; Tserkovnyak, Y.; Tsukamoto, A.; Moriyama, T.; Lee, K.-J.; Ono, T. Fast domain wall motion in the vicinity of the angular momentum compensation temperature of ferrimagnets. *Nat. Mater.* **2017**, *16*, 1187–1192.
- (21) Blasing, R.; Ma, T.; Yang, S.-H.; Garg, C.; Dejene, F. K.; N'Diaye, A. T.; Chen, G.; Liu, K.; Parkin, S. S. P. Exchange coupling torque in ferrimagnetic Co/Gd bilayer maximized near angular momentum compensation temperature. *Nat. Commun.* **2018**, *9*, 4984.
- (22) Pai, C.-F.; Liu, L.; Li, Y.; Tseng, H. W.; Ralph, D. C.; Buhrman, R. A. Spin transfer torque devices utilizing the giant spin Hall effect of tungsten. *Appl. Phys. Lett.* **2012**, *101*, 122404.
- (23) Liu, L.; Pai, C.-F.; Li, Y.; Tseng, H. W.; Ralph, D. C.; Buhrman, R. A. Spin-torque switching with the giant spin Hall effect of tantalum. *Science* **2012**, *336*, 555–558.
- (24) Hao, Q.; Xiao, G. Giant spin Hall effect and switching induced by spin-transfer torque in a W_xCo₄₀Fe₄₀B₂₀/MgO structure with perpendicular magnetic anisotropy. *Phys. Rev. Applied* **2015**, *3*, 034009.
- (25) Ryu, K.-S.; Thomas, L.; Yang, S.-H.; Parkin, S. Chiral spin torque at magnetic domain walls. *Nat. Nanotechnol.* **2013**, *8*, 527–533.
- (26) Emori, S.; Bauer, U.; Ahn, S.-M.; Martinez, E.; Beach, G. S. D. Current-driven dynamics of chiral ferromagnetic domain walls. *Nat. Mater.* **2013**, *12*, 611–616.
- (27) Thiaville, A.; Rohart, S.; Jue, E.; Cros, V.; Fert, A. Dynamics of Dzyaloshinskii domain walls in ultrathin magnetic films. *EPL (Europhysics Letters)* **2012**, *100*, 57002.
- (28) Martinez, E.; Emori, S.; Perez, N.; Torres, L.; Beach, G. S. D. Current-driven dynamics of Dzyaloshinskii domain walls in the presence of in-plane fields: Full micromagnetic and one-dimensional analysis. *J. Appl. Phys.* **2014**, *115*, 213909.
- (29) Li, P.; et al. *Ultrafast racetrack based on compensated Co/Gd-based synthetic ferrimagnet with all-optical switching*; 2022, arXiv:2204.11595 [cond-mat.mes-hall], arXiv, DOI: 10.48550/arXiv.2204.11595 (accessed on May 4, 2022).
- (30) Maccariello, D.; Legrand, W.; Reyren, N.; Garcia, K.; Bouzehouane, K.; Collin, S.; Cros, V.; Fert, A. Electrical detection of single magnetic skyrmions in metallic multilayers at room temperature. *Nat. Nanotechnol.* **2018**, *13*, 233–237.
- (31) Woo, S.; Song, K. M.; Zhang, X.; Ezawa, M.; Zhou, Y.; Liu, X.; Weigand, M.; Finizio, S.; Raabe, J.; Park, M.-C.; Lee, K.-Y.; Choi, J. W.; Min, B.-C.; Koo, H. C.; Chang, J. Deterministic creation and deletion of a single magnetic skyrmion observed by direct time-resolved x-ray microscopy. *Nature Electronics* **2018**, *1*, 288–296.
- (32) Buttner, F.; Lemesh, I.; Schneider, M.; Pfau, B.; Gunther, C. M.; Hessing, P.; Geilhufe, J.; Caretta, L.; Engel, D.; Kruger, B.; Viehaus, J.; Eisebitt, S.; Beach, G. S. D. Field-free deterministic ultrafast creation of magnetic skyrmions by spin-orbit torques. *Nat. Nanotechnol.* **2017**, *12*, 1040–1044.
- (33) Je, S.-G.; Vallobra, P.; Srivastava, T.; Rojas-Sanchez, J.-C.; Pham, T. H.; Hehn, M.; Malinowski, G.; Baraduc, C.; Auffret, S.; Gaudin, G.; Mangin, S.; Bea, H.; Boulle, O. Creation of magnetic skyrmion bubble lattices by ultrafast laser in ultrathin films. *Nano Lett.* **2018**, *18*, 7362–7371.
- (34) Buttner, F.; Pfau, B.; Bottcher, M.; Schneider, M.; Mercurio, G.; Gunther, C. M.; Hessing, P.; Klose, C.; Wittmann, A.; Gerlinger, K.; Kern, L.-M.; Struber, C.; von Korff Schmising, C.; Fuchs, J.; Engel, D.; Churikova, A.; Huang, S.; Suzuki, D.; Lemesh, I.; Huang, M.; Caretta, L.; Weder, D.; Gaida, J. H.; Moller, M.; Harvey, T. R.; Zayko, S.; Bagschik, K.; Carley, R.; Mercadier, L.; Schlappa, J.; Yaroslavtsev, A.; Le Guyader, L.; Gerasimova, N.; Scherz, A.; Deiter, C.; Gort, R.; Hickin, D.; Zhu, J.; Turcato, M.; Lomidze, D.; Erdinger, F.; Castoldi, A.; Maffessanti, S.; Porro, M.; Samartsev, A.; Sinova, J.; Ropers, C.; Mentink, J. H.; Dupe, B.; Beach, G. S. D.; Eisebitt, S. Observation of fluctuation-mediated picosecond nucleation of a topological phase. *Nat. Mater.* **2021**, *20*, 30–37.
- (35) Wang, Z.; Guo, M.; Zhou, H.-A.; Zhao, L.; Xu, T.; Tomasello, R.; Bai, H.; Dong, Y.; Je, S.-G.; Chao, W.; Han, H.-S.; Lee, S.; Lee, K.-S.; Yao, Y.; Han, W.; Song, C.; Wu, H.; Carpentieri, M.; Finocchio, G.; Im, M.-Y.; Lin, S.-Z.; Jiang, W. Thermal generation, manipulation and thermoelectric detection of skyrmions. *Nature Electronics* **2020**, *3*, 672–679.
- (36) Tomasello, R.; Martinez, E.; Zivieri, R.; Torres, L.; Carpentieri, M.; Finocchio, G. A strategy for the design of skyrmion racetrack memories. *Sci. Rep.* **2015**, *4*, 6784.
- (37) Jiang, W.; Zhang, X.; Yu, G.; Zhang, W.; Wang, X.; Benjamin Jungfleisch, M.; Pearson, J. E.; Cheng, X.; Heinonen, O.; Wang, K. L.; Zhou, Y.; Hoffmann, A.; te Velthuis, S. G. E. Direct observation of the skyrmion Hall effect. *Nat. Phys.* **2017**, *13*, 162–169.
- (38) Dohi, T.; DuttaGupta, S.; Fukami, S.; Ohno, H. Formation and current-induced motion of synthetic antiferromagnetic skyrmion bubbles. *Nat. Commun.* **2019**, *10*, 5153.
- (39) Hirata, Y.; Kim, D.-H.; Kim, S. K.; Lee, D.-K.; Oh, S.-H.; Kim, D.-Y.; Nishimura, T.; Okuno, T.; Futakawa, Y.; Yoshikawa, H.; Tsukamoto, A.; Tserkovnyak, Y.; Shiota, Y.; Moriyama, T.; Choe, S.-B.; Lee, K.-J.; Ono, T. Vanishing skyrmion Hall effect at the angular momentum compensation temperature of a ferrimagnet. *Nat. Nanotechnol.* **2019**, *14*, 232–236.